Oceanologia, uncorrected, in press
Polish Academy of Sciences
Institute of Oceanology

https://doi.org/10.5697/...

Barrier layer formation and dynamics in the Red Sea based on Argo profiles and sea level anomaly analysis

Hadeel A. Alsayed[1], Mohammed A. Alsaafani[1,2,*], Turki M. Alraddadi[1]

Abstract

This study presents the first comprehensive investigation of the barrier layer (BL) in the Red Sea (RS) based on Argo float observations from 2012 to 2018, combined with sea level anomaly (SLA) data. The BL is defined as the layer between the temperature-based mixed layer (MLT) and the density-based mixed layer (MLD). The RS is divided into three regions – north (26°N–22°N), central (22°N–18°N), and south (18°N–14°N) – to analyze the spatial and temporal variability of the BL. The results show strong evidence of BL presence in all three regions during winter, with maximum thickness observed in January–February, decay by April, and almost no BL during summer. The BL is thickest in the north due to winter cooling and convection, with salinity stratification deepening the MLT below the MLD. It is more moderate and persistent in the central basin, and thinner and short-lived in the south. Buoyancy frequency and salinity analysis confirm that haline stratification stabilizes the water column and sustains the barrier layer. SLA data were used to examine the impact of mesoscale eddies, indicating that anticyclonic eddies (AEs) enhance BL thickness through convergence and downwelling, whereas cyclonic eddies (CEs) tend to erode the BL by shoaling the mixed layer. In the northern RS, unusual deep mixed layers sometimes occur within CEs, which is consistent with the convective overturning during winter. These findings provide the first description of BL characteristics, which improve our understanding of Red Sea upper ocean dynamics, vertical mixing, and climate interactions.

Keywords

Barrier layer; Argo floats; Red Sea; Deep convection; Mixed layer

[1]*Department of Marine Physics, Faculty of Marine Sciences, King Abdulaziz University, P.O. Box 80207, Jeddah 21589, Saudi Arabia.*
[2]*Department of Environmental Sciences, Faculty of Petroleum and Natural Science, Sana'a University, Sana'a, Yemen*
***Correspondence**: malsaafani@kau.edu.sa (M. A. Alsaafani)

Received: 6 May 2025; **revised:** 7 January 2025; **accepted**: 18 January 2026

1. Introduction

The vertical stratification of the ocean reveals three distinctive layers: the surface layer or mixed layer (ML), the thermocline, and the deep layer. The mixed layer serves as an interface between the atmosphere and the underlying ocean, where active mixing processes lead to relatively uniform physical properties. However, the most substantial vertical gradients in properties such as temperature and salinity typically occur beneath the mixed layer, within the thermocline, which acts as a transition to the deeper layer (Sprintall and Cronin, 2001; Kantha and Clayson, 2003). Of particular interest within the surface layer is the barrier layer (BL), which acts as a separator between the surface mixed layer and the thermocline. This division results in the splitting of the mixed layer into two distinct layers: the surface mixed layer and an underlying layer of homogeneously warm water, referred to as the isothermal layer (Sprintall and Cronin, 2001). The thickness of the BL is defined as the difference between the depth of the isothermal layer (i.e., the temperature-based mixed layer MLT) and the density-based mixed layer depth (MLD), also known as the isopycnic layer. The BL has the same properties as the surface layer but a higher density. Salinity-driven stratification is responsible for BL formation. Extensive research efforts have been dedicated to investigating BL formation mechanisms and exploring their spatial and temporal variability. Studies in the western Pacific Ocean showed variation between the depths of the isothermal and isopycnic layers (Lukas and Lindstrom, 1991), whereas a global analysis conducted by Sprintall and Tomczak (1992) using the World Ocean Atlas (Levitus, 1982) provided valuable insights into the BL across the tropical oceans. They developed a high-resolution climatology that revealed seasonal variations in BLT and improved ML depth estimates. Their work advanced the understanding of how BL modulates vertical mixing and stratification across seasons.

Subsequent studies by De Boyer Montegut et al. (2007) and Mignot et al. (2007) expanded this research to cover the global ocean. Mignot et al. (2009) introduced an enhanced global BLT climatology, incorporating a modified calculation method called 'porosity' to account for observed variations. These studies highlight the importance of salinity in ocean dynamics, introduce the (BL) concept, and discuss efforts to characterize its global thickness and distribution.

The BL formation mechanism has been investigated in several studies; Cronin and McPhaden (2002) outlined four BL formation mechanisms in the tropical Pacific Ocean, including horizontal advection, tilting, stretching, and rainfall. Maes and Belamari (2011) suggested that the BL emerges as a result of a tilting-shearing mechanism in response to westerly winds. Additionally, Zeng and Wang (2017) discussed BL formation within three systems: the flux system, the combined system, and the wind system. Furthermore, the subduction of high-salinity waters can lead to the development of shallow salinity stratification that forms BL (Thadathil et al., 2008). Additionally, Rudzin et al. (2017) examined BL formation in eddy regimes and found that warm-core eddies in the eastern Caribbean Sea can develop a BL, which reduce vertical mixing and traps heat in the upper ocean. This structure may impact tropical cyclone intensity by limiting cooling in the ocean surface layer during storms. Pan et al. (2019) provided a detailed analysis of BL features and formation mechanisms in the tropical Pacific Ocean. They documented its evolution across various El Niño-Southern Oscillation events and highlighted the persistent challenges associated with understanding and predicting BL dynamics. Several studies, such as Qu and Meyers (2005) and De Boyer Montegut et al. (2007), have explored BL formation mechanisms related to the horizontal advection of freshwater from local precipitation or the influence of monsoon currents, as observed by George et al. (2019), Thadathil et al. (2007), Shenoi et al. (2004), and Cronin and McPhaden (2002). Regions with major estuaries, such as the Amazon River, exhibit strong BL signatures, as reported by Silva et al. (2005) and Pailler et al. (1999).

BL influences the upper-ocean thermal balance by modifying the vertical heat flux at the base of the ML, trapping heat in the surface layer and inhibiting vertical mixing with the underlying thermocline (Mignot et al., 2009; Lukas and Lindstrom, 1991; Sprintall and Tomczak, 1992). Since the BL temperature closely matches that of the ML, it restricts vertical heat transfer, thereby affecting the seasonal cycle of sea surface temperature and sea surface salinity, and intensifying the effects of hurricanes and cyclones in regions with significant BL thickness (BLT) (Pathirana et al., 2017; Foltz and McPhaden, 2008; Dong et al., 2015; Echols and Riser, 2020; Balaguru et al., 2011, 2012). The (BL) also impacts marine ecosystems, limiting the upward transport of cold, nutrient-rich waters necessary for phytoplankton growth (Mackey et al., 1995; Radenac and Rodier, 1996; Radenac et al., 2013; Ruardij et al., 1997; Cabrera et al., 2011).

The Red Sea represents a unique marine ecosystem strongly influenced by the distinct environmental, geographical and climatic conditions surrounding it. This region is characterized by limited-precipitation, high evaporation rates, and pronounced temperature variability. The wind exhibits strong seasonality, with wind flowing along the Red Sea axis from north-northwest across most of the basin during summer,-whereas in winter the wind direction reverses in the southern region flowing from south-southeast (Bower and Farrar, 2015; Alsaafani and Shenoi, 2004 and Aboobacker et al., 2017).

Circulation in the Red Sea is influenced by wind stress, buoyancy forcing, and seasonal thermohaline variability, resulting in a reversing exchange system (Morcos, 1970; Edwards and Head, 1987; Zhai, 2013). Wind forcing induces southeasterly surface water flow in summer, while the monsoon drives surface waters from the Gulf of Aden into the Arabian Sea. During winter, the flow pattern in the southern Red Sea and Gulf of Aden reverses due to the northeasterly monsoonal winds over the Gulf of Aden, leading to westward flow in the Gulf and enhanced surface inflow into the Red Sea. These variations produce a distinct circulation exchange structure, characterized by a two-layered pattern in winter and a three-layered pattern in summer, promoting the inflow of nutrient-rich waters from the Gulf of Aden into the southern Red Sea (Murray and Johns, 1997; Alsaafani and Shenoi, 2004; Zhai, 2013; Sofianos and Johns, 2015). The Red Sea density structure exhibits pronounced spatial and temporal variability driven by temperature and salinity changes. Surface salinity ranges approximately from 36.5 PSU in the south to 41 PSU in the north. February records the lowest sea surface temperatures, reaching approximately 17.5°C near the Gulf of Suez, approximately 22°C in the northern Red Sea and 27°C in the southern basin. By late June, sea surface temperatures exceed 28°C in the north and peak above 31°C in the southern basin until September (Morcos, 1970; Edwards and Head, 1987; Zhai, 2013).

This study aims to identify the presence and characteristics of the BL in the Red Sea basin, addressing gaps left by previous investigations. Specifically, this research examines the formation, erosion, seasonal variability, spatial distribution, and thickness of the BL within the Red Sea. The findings of this study provide valuable insights into the oceanographic features of the Red Sea, underscoring the importance and uniqueness of investigating BL dynamics in this region. The paper is organized as follows: Section 2 outlines data and methodology, Section 3presents the results and discussion, and Section 4 concludes the paper.

2. Data and methodology

2.1 Data

This study identified 11 Argo buoys in the Red Sea, and their profiles were obtained from the Coriolis Data Center (http://www.coriolis.eu.org/Data-Products/Data-Delivery/Data-selection). The data were carefully extracted from NETCDF files for each Argo buoy and subjected to a rigorous quality assurance process. This extensive quality control process resulted in the selection of five Argo floats that provided high-quality and reliable hydrographic information (Table 1). Temperature and salinity profiles were collected from five Argo floats between 2012 to 2018, with measurements acquired every 2 to 4 days allowing seasonal variability to be examined.

To analyze the impact of mesoscale eddies on the BL, this study utilized sea level anomaly (SLA) data from the Copernicus Marine Service for the period corresponding to the Agro float observations (2016–2018) (https://doi.org/10.48670/moi-00148). The altimeter-derived gridded SLA data were computed relative to 20-years mean (1993–2012) and have a spatial resolution of 0.25° × 0.25° and a daily temporal resolution.

2.2 Methodology

This study focuses on analyzing the vertical structure of the upper ocean in the Red Sea. The Red Sea is divided into three regions: Northern (26°N to 22°N), central (22°N to 18°N), and southern (18°N to 14°N) (Figure 1). Langodan et al. (2017) described this division based on the distinct climatic conditions and events unique to each region.

BLT was calculated following De Boyer Montegut et al. (2007) as the difference between the temperature-based MLT and the density-based MLD (Equation 1). For this analysis, the upper 300 m of each profile were used, as the mixed layer in the Red Sea is almost always shallower than this depth. The reference depth for mixed layer estimation was set to 10 m, deep enough to minimize near-surface variability while remaining shallow enough to represent local sea surface temperature and salinity.

Several temperature thresholds were tested to define MLT and MLD at the Argo float locations. The calculations were repeated with thresholds of 0.2, 0.5, 0.8 and 1.0°C relative to the temperature at 10 m. The 0.2°C threshold often produced MLT and MLD that differed by less than 5 m, even in profiles that exhibited a clearly stratified layer beneath the mixed layer, which led to systematic underestimation of BLT. In contrast, thresholds larger than 0.5°C yielded unrealistically deep MLT values and excessively thick BLs that were inconsistent with the depth range of strong salinity stratification and with previous estimates of winter mixed layer depth in the Red Sea. A threshold of 0°C provided MLT and MLD values most consistent with visual inspection of the profiles and with published mixed layer depths in this region, and this value is also commonly

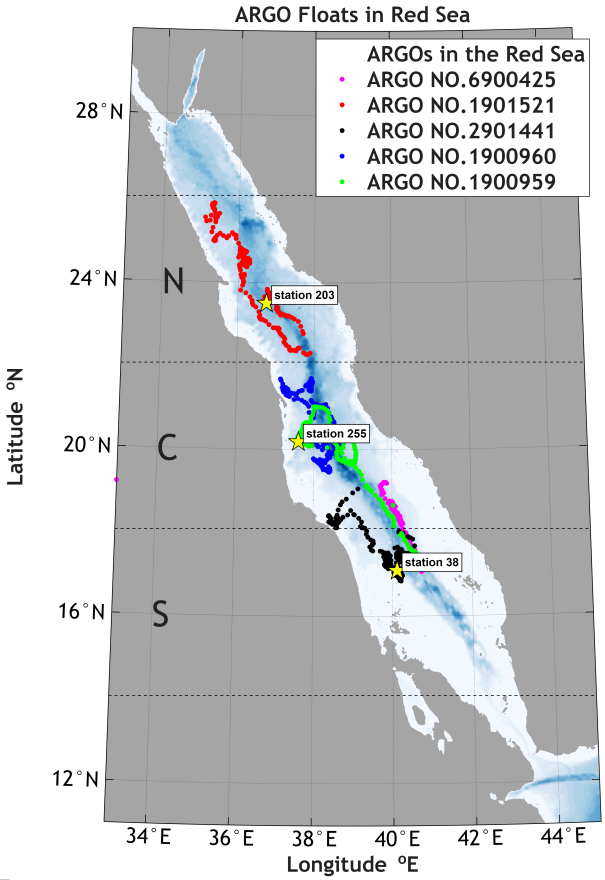

Figure 1. Argo float trajectories in the Red Sea with dashed lines indicating the three regions. The locations of stations 203, 255, and 38 are marked on the map.

Table 1. Argo floats used in this study, showing their temporal coverage and the number of profiles before and after quality control.

Argo No.	Period	Location	Number of profiles before quality control	Number of profiles after quality control
1900959	April 2015–December 2018	Central–South	337	329
2901441	October 2012–July 2014	South–Central	173	173
1901521	November 2015–December 2018	North	277	277
6900425	April 2016–December 2018	South–Central	229	229
1900960	April 2015–December 2018	Central	262	262

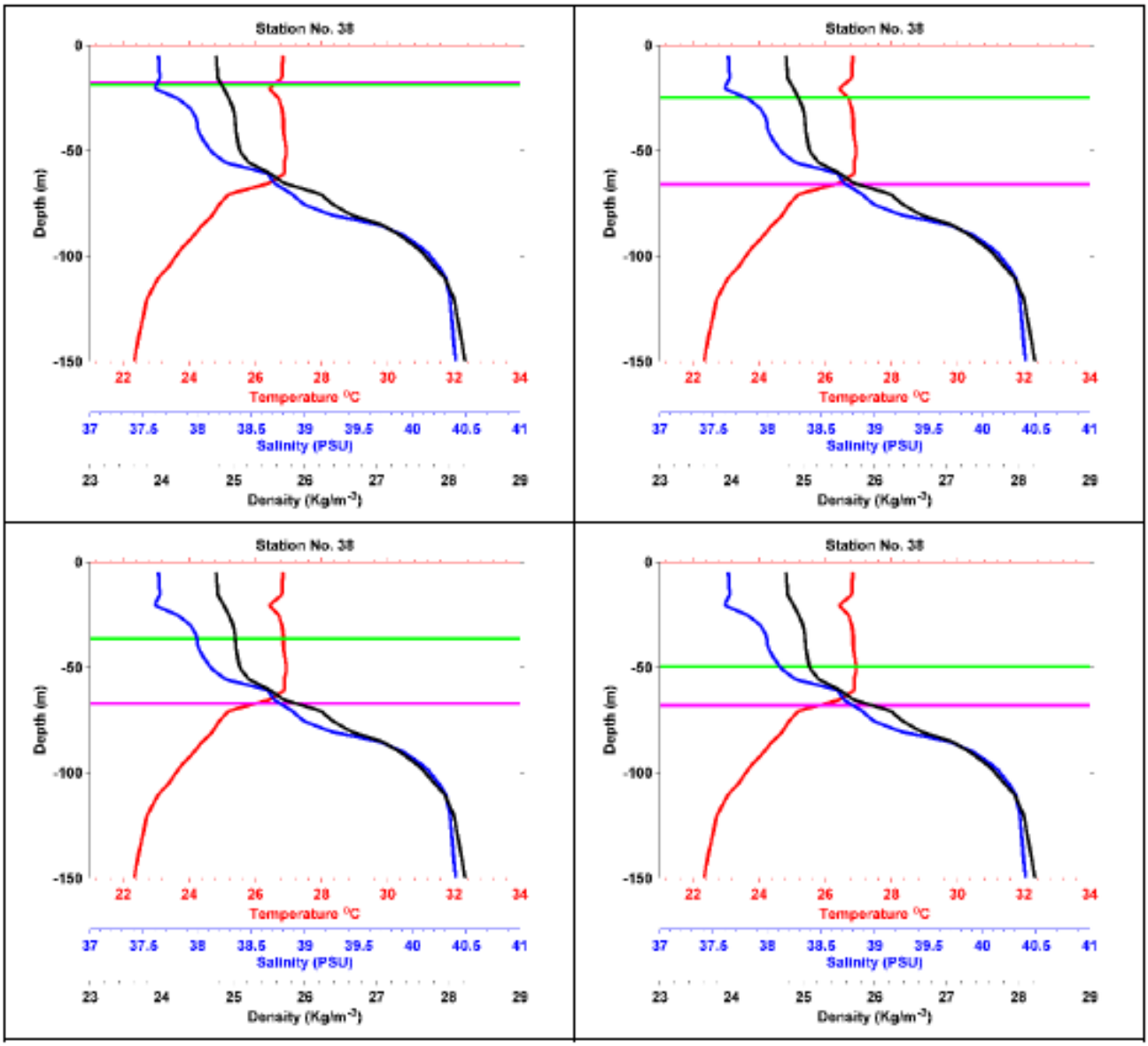

Figure 2. Sensitivity test illustrating the effect of different temperature thresholds (0.2, 0.5, 0.8, and 1°C) on MLT and MLD estimation.

adopted in global BL studies. A temperature difference of 0.5°C was therefore used to define both MLT and MLD in all subsequent analyses. An example of the sensitivity analysis for the different thresholds is presented in Figure 2.

In this framework MLD is defined as the depth at which potential density has increased relative to its value at 10 m by an amount equivalent to a cooling of 0.5°C (Equation 2; Sprintall and Tomczak, 1992), whereas MLT is defined as the depth at which temperature is 0.5°C lower than the value at 10 m (Equation 3). The BLT is given by Equation (1). When the effect of salinity on density stratification is weak, MLD and MLT are nearly identical, and BLT approaches zero.

$$\mathrm{BLT} = \mathrm{MLT} - \mathrm{MLD} \tag{1}$$

$$\mathrm{MLD} = \mathrm{depth} \quad \text{where} \quad \sigma\theta = \sigma\theta_{10\mathrm{m}} + \Delta\sigma\theta \tag{2}$$

where

$$\Delta\sigma\theta = \sigma\theta(\theta_{10\mathrm{m}} - 0.5°\mathrm{C}, \mathrm{S}_{10\mathrm{m}}, \mathrm{P}) - \sigma\theta(\theta_{10\mathrm{m}}, \mathrm{S}_{10\mathrm{m}}, \mathrm{P})$$

$$\mathrm{MLT} = \mathrm{depth} \quad \text{where} \quad \theta = \theta_{10\mathrm{m}} - 0.5°\mathrm{C} \tag{3}$$

where $\sigma\theta$ denotes the potential density, θ denotes potential temperature, S denotes salinity, and P denotes pressure. To characterize the stability of the upper water column, the buoyancy frequency (Brunt-Väisälä frequency) N^2, was computed from the vertical density gradient following Maes and O'Kane (2014) and George et al. (2019).

N^2 is particularly significant in the context of the BL in the ocean. High values of N^2 indicate strong stability in the water column, facilitating BL formation and maintenance. To illustrate the contribution of salinity, N^2 was decomposed into a temperature controlled part, N_T^2, and a salinity controlled component, N_S^2.

$$N^2 = \frac{g}{\rho}\frac{\partial \rho}{\partial z} \approx \left(g\alpha\frac{\partial T}{\partial z} - g\beta\frac{\partial S}{\partial z}\right)$$

$$N^2 = N_T^2 + N_S^2 \tag{4}$$

where,

$$\alpha = \rho^{-1}\frac{\partial \rho}{\partial T}, \quad \beta = \rho^{-1}\frac{\partial \rho}{\partial S}$$

$$N_T^2 = g\alpha\frac{\partial T}{\partial z}$$

$$N_S^2 = N^2 - N_T^2$$

Here, β is the haline contraction coefficient, α is the thermal expansion coefficient, g is gravitational acceleration, ρ is seawater density, T is temperature, S is salinity, and z is depth.

The term N_T^2 reflects the contribution of temperature alone, and N_S^2 represents the additional contribution of salinity to the total N^2. The difference between N^2 and N_T^2 thus gives N_S^2 and identifies the depths where salinity stratification stabilizes the water column. In the figures N^2 and N_S^2 are plotted, with N_S^2 used in particular to highlight the depth range where haline stratification is strongest, and BL formation occurs.

3. Results and discussion

3.1 Barrier layer detection in the Red Sea

To estimate BLT, salinity, temperature, and density profiles from all Argo floats in the northern, central, and southern regions of the Red Sea were organized by year and further categorized into seasons: fall, winter, spring, and summer. Monthly mean profiles were derived from those individual profiles to estimate the monthly thickness of the BL in the Red Sea. Figure 3 shows the time series of monthly BLT derived from the five selected Argo floats, indicating the presence of the BL. The peaks represent the maximum BL thickness, which is notably present during the winter months from December to February. The presence of the BL was observed in all three regions.

In all regions of the Red Sea, BL formation begins in November–December and reaches its maximum thickness in January–February. Beginning in March BL thickness de-

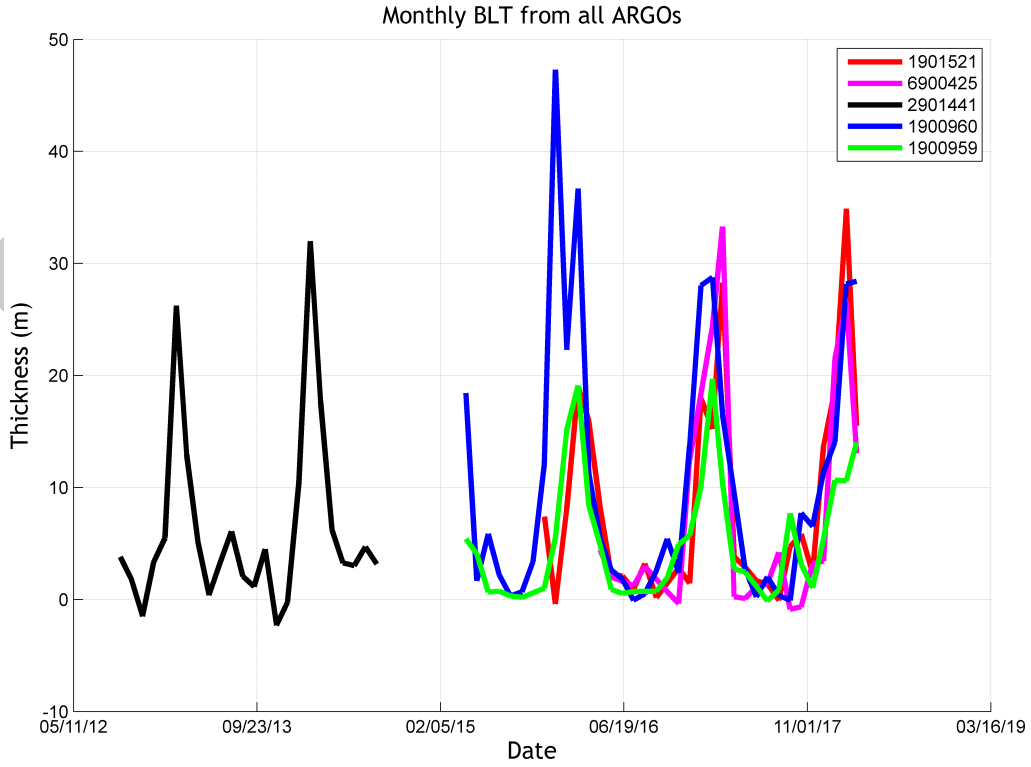

Figure 3. Monthly mean BLT for the period 2012–2018 derived from all available Agro floats in the Red Sea.

creases gradually, reaching its minimum value of approximately 10 m, in April. By May, the BL vanishes and remains absent throughout the summer months until September. In the southern region, evidence of BL presence is observed during September (Figure 3).

The following sections investigate BL formation and decay using Argo floats profiles collected between 2012 and 2018 to examine presence of BL across three regions. The 2017–2018 profiles were used for the northern and central regions starting from October 2017. For the southern region, the 2012–2013 profiles were used due to a lack of Argo data for the later period.

3.2 Northern Red Sea

To visualize water-column characteristics throughout the year, contour plots of temperature, salinity, density, N^2, and N_S^2 were generated for all seasons. For clarity, only figures corresponding to the winter season are presented here. Additionally, multi-axis profiles of temperature, salinity, and density were constructed for the winter season, highlighting the thickness of the BL.

3.2.1 BL formation phase during autumn (October–November 2017)

During this season sea surface temperature ranges between 27°C to 30°C, while salinity gradually increases from 39.5 to 40.5 PSU. The temperatures remain nearly uniform

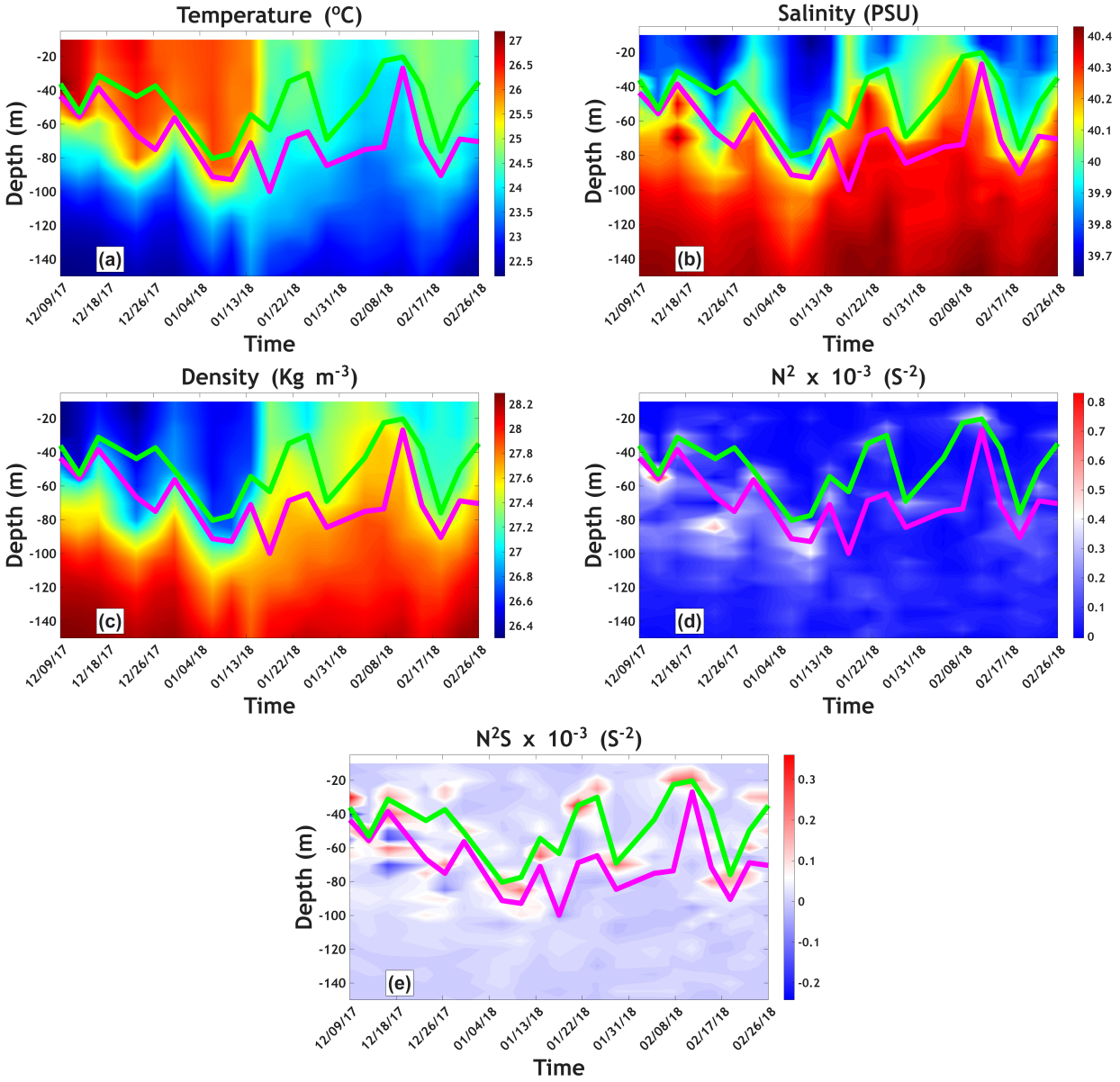

Figure 4. Vertical distribution of temperature (a), salinity (b), density (c), N^2 (d) and N_S^2 (e) during winter 2017–2018 (December–February) in the northern region. The magenta line represents MLT and the green line represents MLD.

up to a depth of 50 m, salinity remains uniform from the surface to approximately 40 m , whereas the MLD varies around 50 m. By the end of November, a BL formed marked by salinity at approximately 0.2 PSU higher than surface values and a gradual temperature decrease. In November, the BL persists only briefly, likely due to continued deepening of the MLD driven by the wintertime convective process (Figure S1). A more persistent BL is observed by the mid-December, discussed in the following section. MLD deepening is driven by the increased water column density with decreasing temperature, consistent with previous findings (Krokus et al., 2021). According Langodan et al. (2017) and Krokus et al. (2021) wind input decreases during early autumn, and surface buoyancy loss in the Red Sea is primarily driven by surface cooling. Furthermore, previous reports stated that the correlation between buoyancy flux and ML depth increases overall, with the deepest ML occurring in regions experiencing the greatest buoyancy fluxes.

3.2.2 The growth phase during winter (December–February) 2018

Figure 4 shows the temperature, salinity and density sections during winter, with MLD and MLT marked through the period and, deepening to a maximum of approximately 100 m MLT and 90 m for MLD. The BLT represents the differences between the MLT (magenta) and MLD (green). BL formation began in mid-December 2017 and intensified until mid-February 2018, reaching a maximum thickness of approximately 50 m in February. The influence of salinity stratification is described in the N^2–N_S^2 Section (Figure 4d and e), where elevated N_S^2 coincides with the maximum extent of the MLD relative to total N^2.

During this season, a rapid temperature decrease from 27°C to 25°C occurs by the end of December, reaching its lowest levels in January and February, where it stabilizes at 24°C. Below the surface, the temperature remains relatively uniform up to a depth of 100–150 m. Surface salinity starts at 39 PSU and gradually increases with depth, reaching 40.2 PSU at a depth of 100 m or greater as shown in Figure 4. This cooling increases the density of the surface layer, resulting in the deepening of the ML. As the surface layer deepens, differences in the deepening rates of MLT and MLD lead to BL formation, as illustrated in Figure 4.

BLT increases from December and reaches its maximum extent by the end of winter, aligning with the maximum MLD depth. These winter changes have a significant impact on the water column. The increased stratified stability can then cause the formation and deepening of the BLT (Shenoi et al., 2004).

In the northern basin, the largest wintertime N_S^2 values occur where MLT lies between approximately 50 and 80 m, corresponding to the depth range in which MLT is below MLD, and BLT, is the largest (Figure 4e). This confirms that BL is associated with enhanced haline stratification rather than temperature alone and that salinity plays a key role in stabilizing the water column at the base of the mixed layer.

During the winter season, particularly in the northern basin, there is significant variability in BL and ML depths. This finding is consistent with previous studies of mixed-layer dynamics, including those by Abdulla et al. (2018) and Krokos et al. (2021). This pronounced variability is attributed to a combination of factors identified in earlier studies, including surface cooling and fresh water loss (buoyancy loss), wind stress, and anticyclone activity.

Specifically, during this period, the dynamics shift from wind-induced mixing to convective processes. Convection triggers the creation of denser water, which decreases stratified stability. The northern basin is characterized by a strengthening anticyclonic eddy during winter, as reported by Zhan et al. (2014) and Zhan et al. (2019), which in turn promotes mixed layer deepening (Gaube et al., 2019). Figure 5 presents the vertical profile of temperature, salinity, and potential density for station 203 during the winter season. The stratification induced by salinity limits the MLD to approximately 20 m, whereas the MLT extends to around 70 m, resulting in a BLT of about 50 meters.

In the northern basin strong wintertime cooling and evaporation produces large surface buoyancy loss and drives deep convection, which increases the mixed layer density. The underlying water masses are influenced by advection and subduction of saltier waters formed farther north, as well as large-scale overturning circulation, thereby maintaining a pronounced salinity increase with depth beneath the mixed layer. As a result, density stratification within the BL depth range is largely controlled by salinity, while temperature remains nearly uniform.

3.2.3 Decay phase during spring (March–April) and summer (May–September), 2018

During the spring season, as temperature continues to rise, strengthened thermal stratification leads to gradual MLD and MLT shoaling across most of the Red Sea compared with winter conditions. Consequently, the BL begins to weaken by mid-spring, and disappears by the end of spring, except for a brief BL formation event at the beginning of April caused by salinity stratification, which decays shortly thereafter (Figure S2). Abdulla et al. (2018) and Krokos et al. (2021) suggest that intensified wind stirring and convective mixing, driven by surface cooling, can penetrate to the top of the thermocline, depending on the mixed layer and potentially eroding preexisting or newly formed BLs. This mechanism explains the disappearance of the BL by late spring as noted by Thadathil et al. (2007), who reported that wind stresses tend to suppress BL formation by enhancing surface turbulent kinetic energy. Thus, the same factors that promote mixed-layer deepening also contribute to BL disappear-

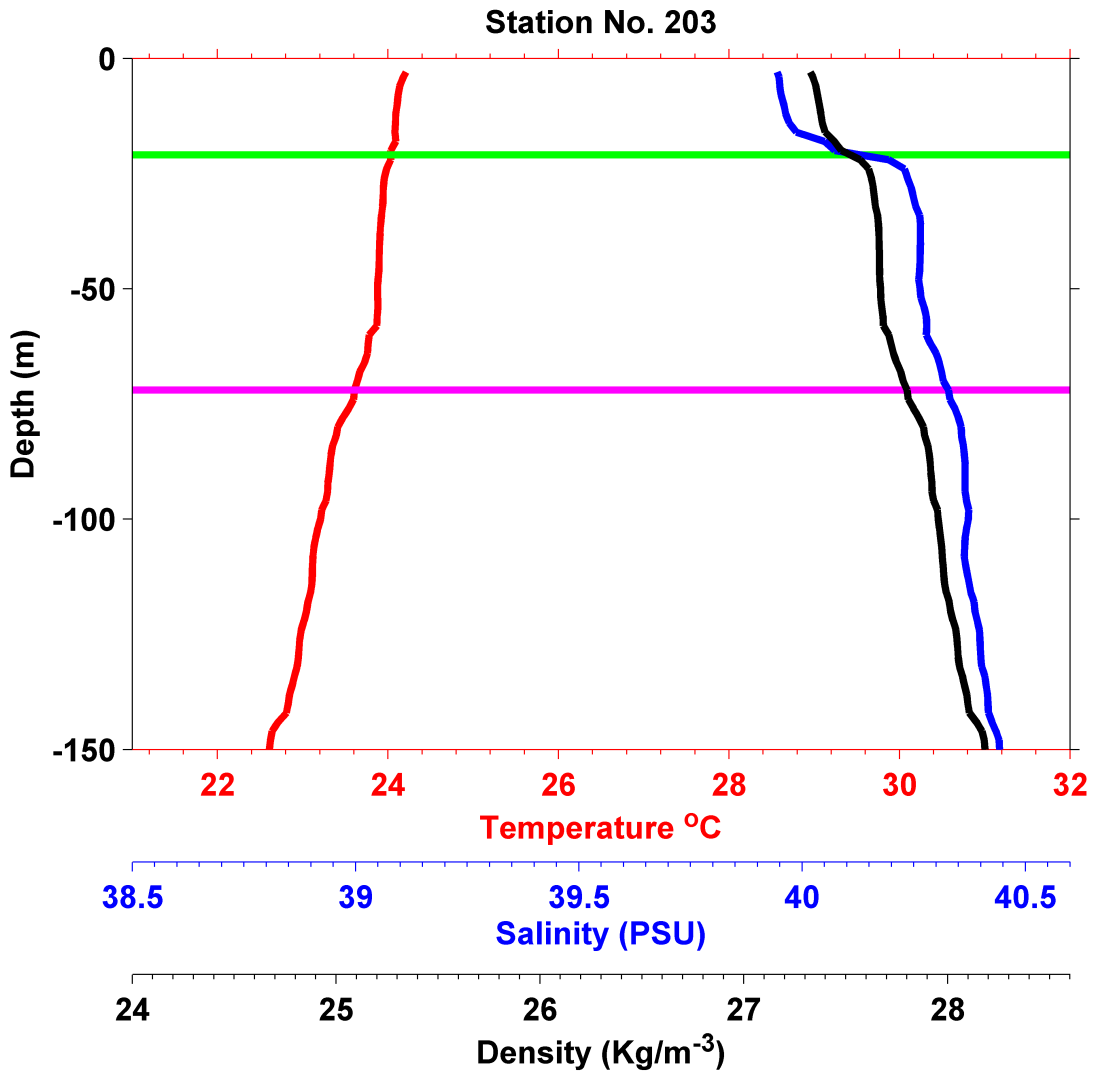

Figure 5. Temperature, salinity, and density profiles for station no. 203 on 8 February 2018 in the northern Red Sea, obtained from Argo 1901521. The MLD represented by green line and magenta for MLT, the BLT is the difference between both lines.

ance. In the summer, the presence of BL is not evident (Figure S3).

3.3 Central Red Sea

3.3.1 Formation phase during autumn (October–November 2017)

The hydrographic structure in the central region during the fall season shows nearly uniform temperature from the surface to a depth of about 50 m with surface temperature of approximately 30–31°C throughout the season. Salinity ranges from 39.5 to 39 PSU over the course of the season, with uniform salinity observed to a depth of 50 m in October deepening to approximately 80 m in November (Figure S4). A thin BL appears during this season with a thickness of approximately 10 m.

A relatively fresh and cold water mass enters the surface layer to a depth of approximately 100 m. These water masses appear in November and exhibit salinity values approximately 0.5 PSU less than the surface salinity, representing Gulf of Aden Surface Water (GASW) entering through the strait. Studies conducted by Zarokanellos et al. (2017) have proven that GASW flows northward into the Red Sea through the Bab al-Mandab Strait, reaching the central region by November. This inflow enhances nutrient levels in the upper layers, supporting biological productivity, with mesoscale eddies further enhancing nutrient distribution through horizontal and vertical transport.

Eddy activity is intense in the central basin, as noted by Zhan et al. (2014, 2019). Those eddies contribute to

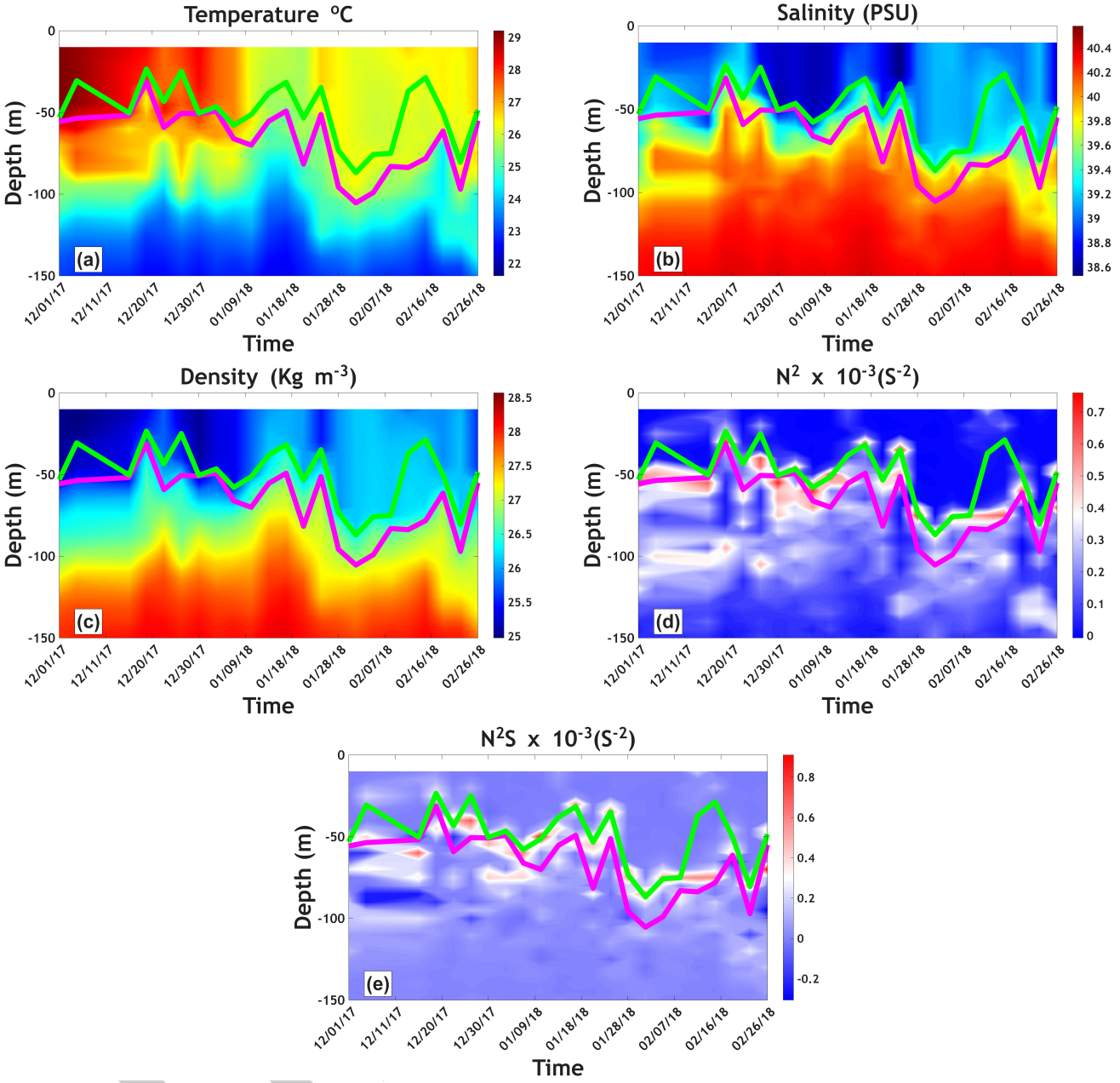

Figure 6. Vertical distributions of temperature (a), salinity (b), N^2 (c), density (d) and N_S^2 (e) during winter 2017–2018 (December–February) in the central region. Magenta line represents MLT, and green line represents MLD.

ML deepening during anticyclonic eddy and shallowing ML during cyclonic eddy (Gaube et al., 2019). The conditions in this region are favorable for BL development, which starts growing by the end of November (Figure not shown). Krokos et al. (2021) and Langodan et al. (2014) showed that during this period the wind pattern shifts toward the winter regime in the southern region (SSE), while northern winds (NNW) still prevail in the central region (18°N–22°N)) and remain relatively weak compared with other seasons. Therefore, during the fall, the effect of buoyancy prevails over the effect of wind. This is one of the factors contributing to the formation of BL.

3.3.2 The growth phase during winter (December–February 2018)

During winter, the temperature remains uniform from the surface to about 50 m and deepens to 100 m by the end of the season. At the BL formation site, salinity differs by about 0.5 PSU from the surface value. During this season, the mixed layer reaches its maximum

depth, extending to 100 m in February (Figure 6). This period exhibits a pronounced difference between MLT and MLD, leading to BL formation and maximum thickness, as salinity stratification limits MLD, with peak MLD depths coinciding with elevated N2 and N_S^2 values. In particular, peaks in N_S^2 are collocated with the depth interval between MLD and MLT, which indicates that the BL in the central basin is maintained by salinity-driven stratification. Figure 7 presents vertical profiles of temperature, salinity, and potential density for station 255 during winter. The MLD reaches about 50 m, while the MLT extends to about 75 m, resulting in a BLT of approximately 25 m.

During this season, northwesterly winds that blow over the northern region and extend into the central basin are particularly strong over the western parts of the basin, as demonstrated by Langodan et al. (2017), leading to increased wind stress (Krokos et al., 2021). Strong winds enhance the presence of cyclonic and anticyclonic eddies in the central basin, which peak during winter (Zhan et al., 2014, 2019). The detected BL becomes thicker in winter compared to fall, providing additional evidence of BL thickening, possibly due to the influence of anticyclonic eddies. Zhan et al. (2014) showed that AEs are more active and stronger during winter compared to CEs.

The combined effects of a decrease in temperature, salinity increase (buoyancy loss), wind stress, and eddy activity lead to BL formation and thickening in the central basin during winter.

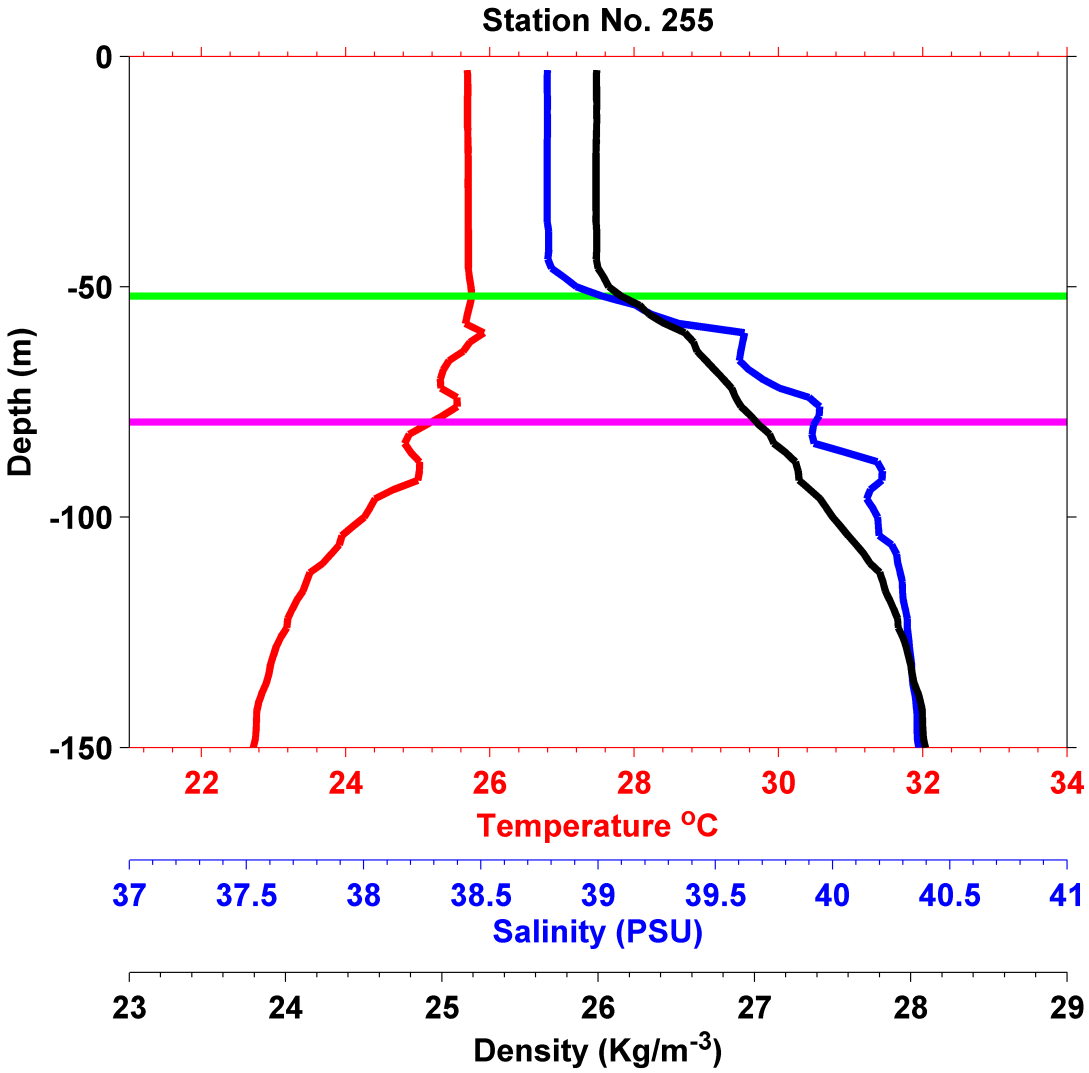

Figure 7. Temperature, salinity, and density profiles for station no.255 on January 21, 2018, in the Central region, obtained from Argo float 1900959. The MLD represented by green line and magenta for MLT, the BLT is the difference between both lines.

Although there is no significant local freshwater input in this region, the observed haline stratification can be explained by basin scale processes. In winter, surface cooling and evaporation increase the density of surface waters and drive convective deepening of the mixed layer. At the same time northward advection of relatively fresh Gulf of Aden Surface Water and the action of anticyclonic eddies trap fresher water above saltier subsurface water that is connected to the overturning circulation in the northern Red Sea. The resulting vertical salinity gradient at the base of the mixed layer is therefore not a purely formal consequence of the chosen temperature threshold. Still, it reflects the underlying water mass structure and circulation.

3.3.3 The decay phase during spring (March–April) and summer (May–September 2018)

In spring, enhanced thermal stratification causes the mixed layer to shoal across the Red Sea. During this period, buoyancy fluxes are weak in the central basin, as reported by Krokos et al. (2021) and Abdullah et al. (2018). As a result, the mixed layer shoals, while the BL begins to erode and

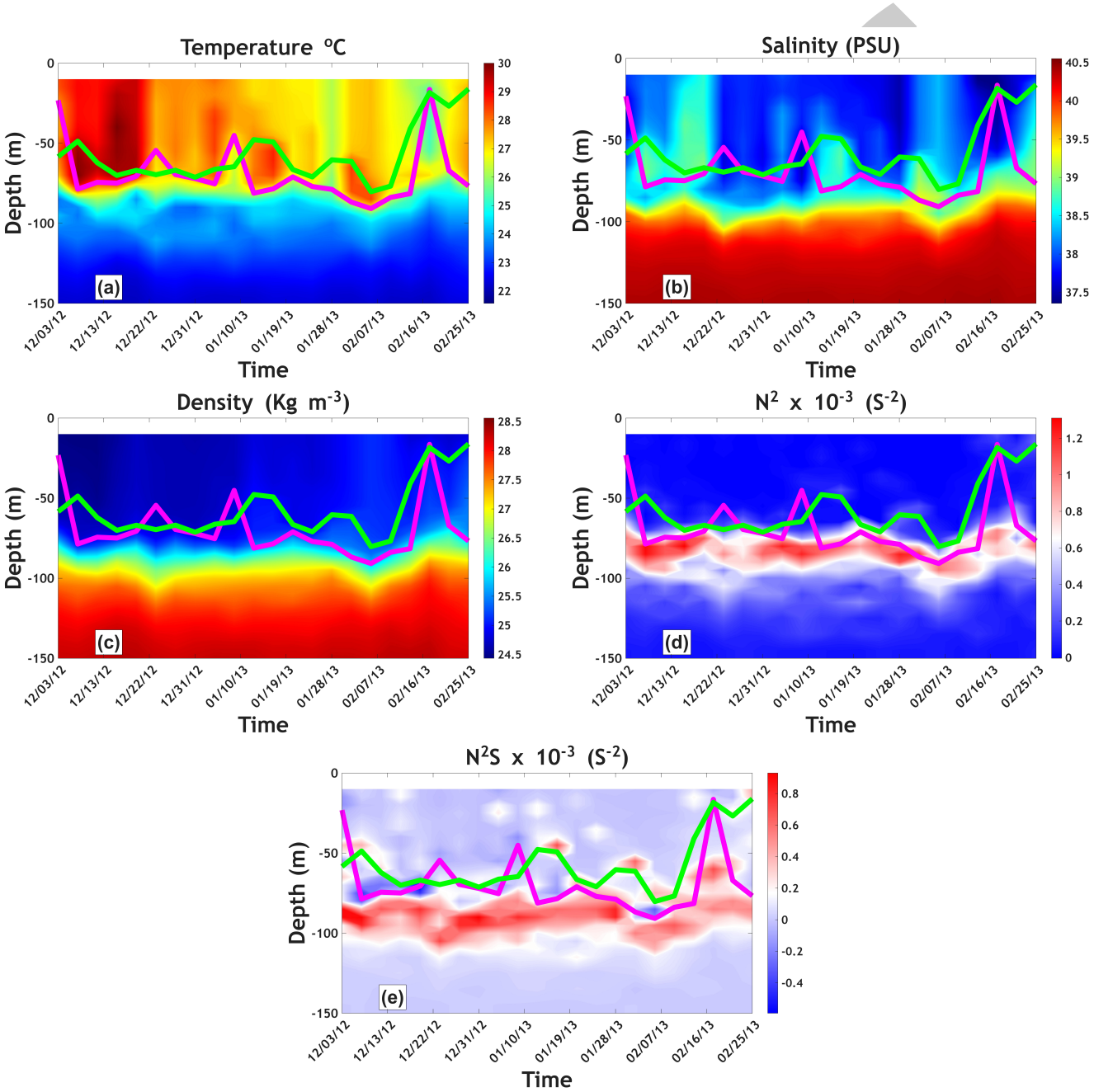

Figure 8. Vertical distribution of temperature (a), salinity (b), N^2 (c) density (d)and N_S^2 (e) during winter 2012–2013 (December–February) in the south region, the magenta line represents MLT. and the green line represents MLD.

gradually disappears by the end of the season (Figure S5). In summer, the BL in the central basin is generally weak or absent due to the relatively shallow ML, which is typically less than 20 m deep and reaches a maximum depth of about 40 m (Figure S6). This shallow ML inhibits the formation of a distinct BL. However, the BL can intermittently appear with a small thickness of approximately 5 m, particularly in association with wind forcing during Tokar Gap events and the transitional wind months, highlighting the dynamic interplay of physical processes in the region.

3.4 Southern Red Sea

3.4.1 Formation phase during autumn (October–November 2012)

In the southern region, Argo floats data were available only from 2012 to 2014, preventing a direct comparison with the northern and central regions for the same year. During fall, surface temperatures range approximately 32°C and 28°C, with relatively homogeneous salinity around 39 to 38 PSU up to 50 m deep. At a depth of approximately 75 m a water mass with a temperature around 20°C and a salinity about 37 PSU was observed, indicating Gulf of Aden Intermediate Water, which enters the Red Sea through the Bab al Mandeb Strait during summer. In contrast to other regions of the Red Sea, the BL in the southern basin is either absent or only weakly developed at the beginning of October, with a thickness of approximately 10 to 15 m (Figure S7).

Previous studies have shown that by mid-September, the exchange between the Red Sea and Gulf of Aden shifts to a winter two-layer system (Sofianos and Johns, 2003; Alsaafani and Shenoi, 2004; Zhai et al., 2013). This transition coincides with a decrease in NNW wind intensity and the onset of SSE wind in the southern region during winter (Langodan et al., 2014). This circulation pattern fully devel-

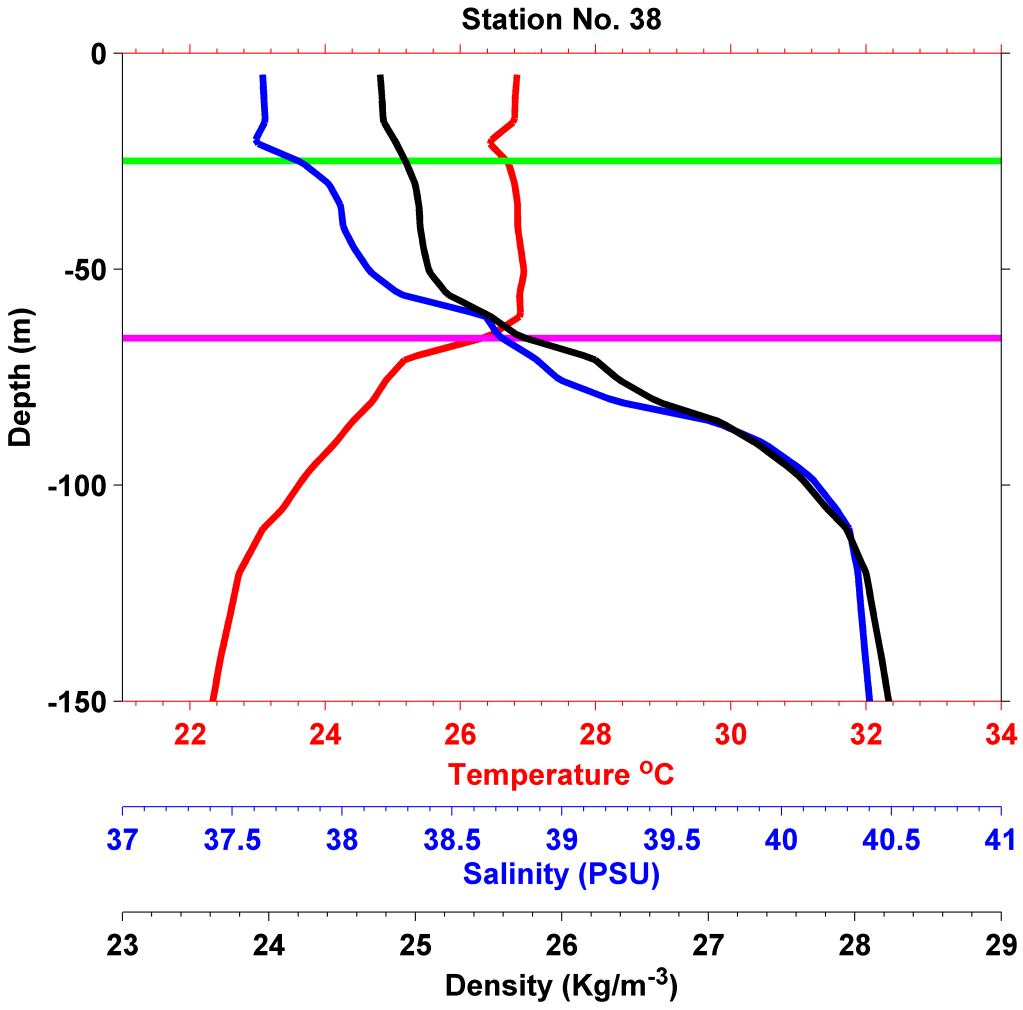

Figure 9. Temperature, salinity, and density profiles for station no. 38 on 21 February 2013 in the southern Red Sea, obtained from Argo 2901441. The MLD represented by green line and magenta for MLT, the BLT is the difference between both lines.

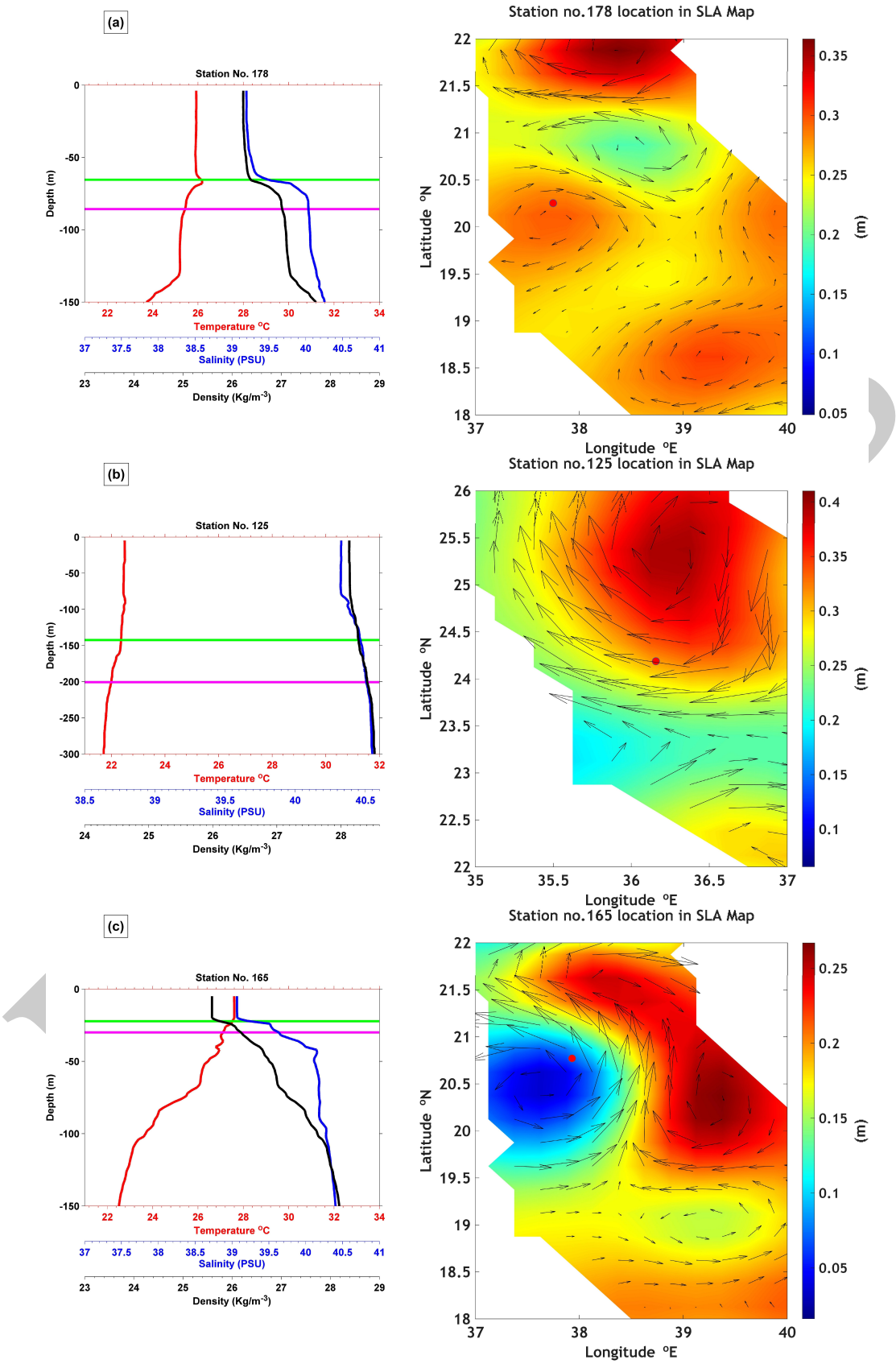

Figure 10. Profiles of temperature, salinity and density from Argo station no. 178 located in the central Red Sea on February 14, 2017 (a), Argo station no. 125 located in the northern Red Sea on February 14, 2017 (b), Argo station no. 165 located in the central Red Sea on February 12, 2017 (c). The magenta line represents MLT, the green line represents MLD, and their difference represents the BL. SLA maps for the same date are plotted to the right of pannels CE and AE. Station locations are indicated by red dots.

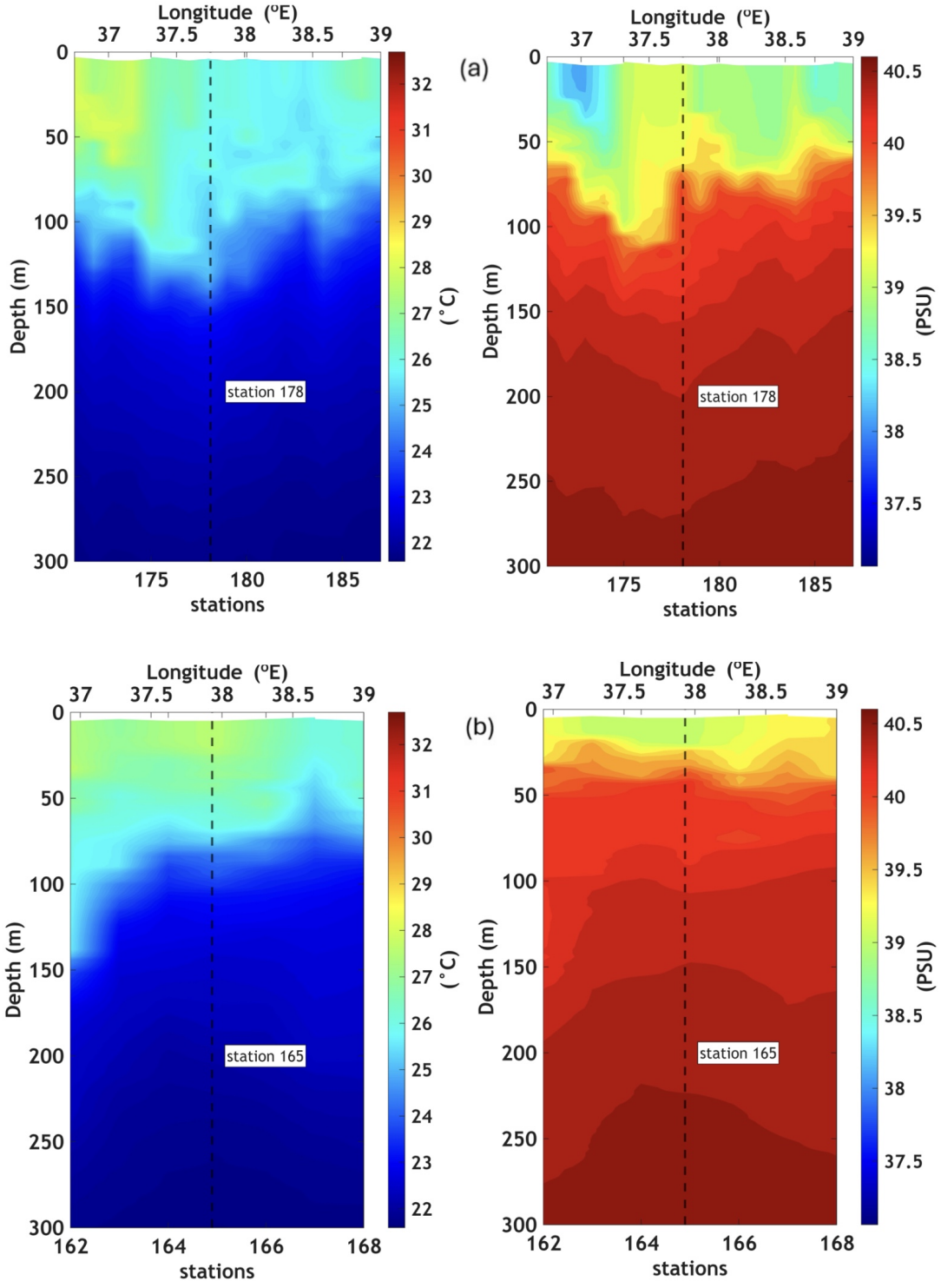

Figure 11. Vertical sections of temperature (left) and salinity (right) in the central region, A dashed line represents station no. 178 location at the AE site (a) and dashed line represents station no. 165 at the CE site (b).

ops in early November and continues until March. during which GASW enters the southern Red Sea as a surface layer from the Gulf of Aden.

3.4.2 The growth phase during winter (December–January 2013)

The BL becomes more pronounced during winter, reaching a thickness exceeding 25 meters by mid-December. BL thickness decreases briefly before reappearing by mid-January and persists until the end of February, as shown in Figure 8. During this season, south-southeasterly (SSE) winds predominate south of 18°N. These winds originate in the Arabian Sea as part of the northeastern monsoon system and enter the Red Sea through the Bab al Mandab Strait (Abdulah et al., 2019; Langodan et al., 2014). Between November and April, NNW winds converge with SSE winds in the southern region, forming a convergence zone around 16–18°N (Langodan et al., 2014; Zhai, 2013). This wind coverage results in surface buoyancy in the central and southern part of the basin, promoting deepening of the ML (Krokos et al., 2021). The low salinity water masses observed during autumn may have advected northward or mixed into the surface layer to depths of up to 100. These mixing processes may result in an increased mixed layer depth, as demonstrated by (Krokus et al., 2021).

Figure 8c shows the combined effects of temperature and salinity on water column stability, while Figure 8(e) demonstrates the role of salinity in stratification. Salinity stratification has a significant impact on the boundary layer, as illustrated in Figure 8e. This stabilization results in a shallower MLD, particularly when salinity gradients are more effective. On the other hand, temperature-driven stratification primarily impacts the MLT. Seasonal variations, such as freshwater influx or evaporation, modulate N^2 and N_S^2 leading to regional and temporal differences in BL across the Red Sea. Overall, salinity-driven stratification plays a more dominant role in shaping BL during this period. At depths between 50 and 100 m as shown in Figure 8c, elevated N^2 values indicate strong stratification influenced by both temperature and salinity gradients which suppress vertical mixing. The maxima of N_{S^2} values are again located between the depths of MLD and MLT, which indicates that the winter BL is supported by the haline gradient between the advected fresher Gulf of Aden Surface Water that enters at the surface and the saltier underlying Red Sea water. Figure 9 presents vertical profiles of temperature, salinity, and potential density for station 38 during winter. The MLD reaches about 25 m, while the MLT extends to about 65 m, resulting in a BLT of approximately 40 m.

3.4.3 Decay phase during spring (March–April) and summer (May–September) 2013

During the spring season, sea surface temperature exhibits a progressive increase from approximately 26.5°C at the beginning of the season to around 29°C by its end. Surface salinity remains relatively constant at about 37.5 PSU. Vertically, within the BL depth range, salinity values increase from approximately 38.5 to 39.5 PSU, indicating a pronounced subsurface salinity gradient that contributes to BL formation and maintenance (Figure 8S). The MLD during spring is shallower than that during winter leading to the formation of a BL with a thickness of approximately 30–35 m, centered near a depth of 50 m. The vertical structure observed in the southern region is strongly influenced by monsoon wind patterns and the region's proximity to the Bab al Mandab Strait.

During this period, the wind field maintains a winter-like pattern but with reduced intensity, characterized by southeasterly flow over the southern Red Sea (Alsaafani and Shenoi, 2004). The predominance of SSE winds during winter drives the inflow of fresher and colder GASW, which plays a key role in increasing (BLT). Similar to the mechanisms described by (Cronin and McPhaden, 2002) in their study on BL formation during westerly wind bursts in the equatorial Pacific, the unique winter conditions in the southern Red Sea – characterized by enhanced surface cooling and freshwater input – create favorable conditions for BL development. In this region, BL formation typically begins in early December and persists through March and April, in alignment with the seasonal evolution of ML.

During summer, the SSE wind system gradually weakens and transitions to NNW winds which prevail along the entire Red Sea (Langodan et al., 2017; Langodan et al., 2014). In addition, surface heat flux increases during this season and the flow of the warm surface layer moves southward. The exchange circulation transforms into a three-layer system, consisting of warm surface outflow, intermediate inflow of fresher colder water, and saline outflow at the bottom (Sofianos and Johns, 2003; Alsaafani and Shenoi, 2004; Krokos et al., 2021). During the summer season the mixed layer is shallow, with a depth of approximately 30 m (Figure 9S), consistent with the findings of Krokus et al. (2021) and Abdullah et al. (2018). These factors contribute to the formation of a temporary BL at the summer's onset, usually less than 15 m thick. However, this temporary BL dissipates as wind intensity decreases and solar heating intensifies, strengthening thermal stratification.

In the central and southern Red Sea some profiles indicate density compensated layers associated with temperature inversions, which may modify vertical exchanges at the base of the mixed layer. However, a detailed investigation of these structures lies beyond the scope of the present study.

3.5 Impact of eddies on the barrier layer

In this section, SLA data are used to examine the influence of anticyclonic (AEs) and cyclonic eddies (CEs) on BL variability with a focus on the central and northern Red Sea during the winter of 2016–2017 and 2017–2018.

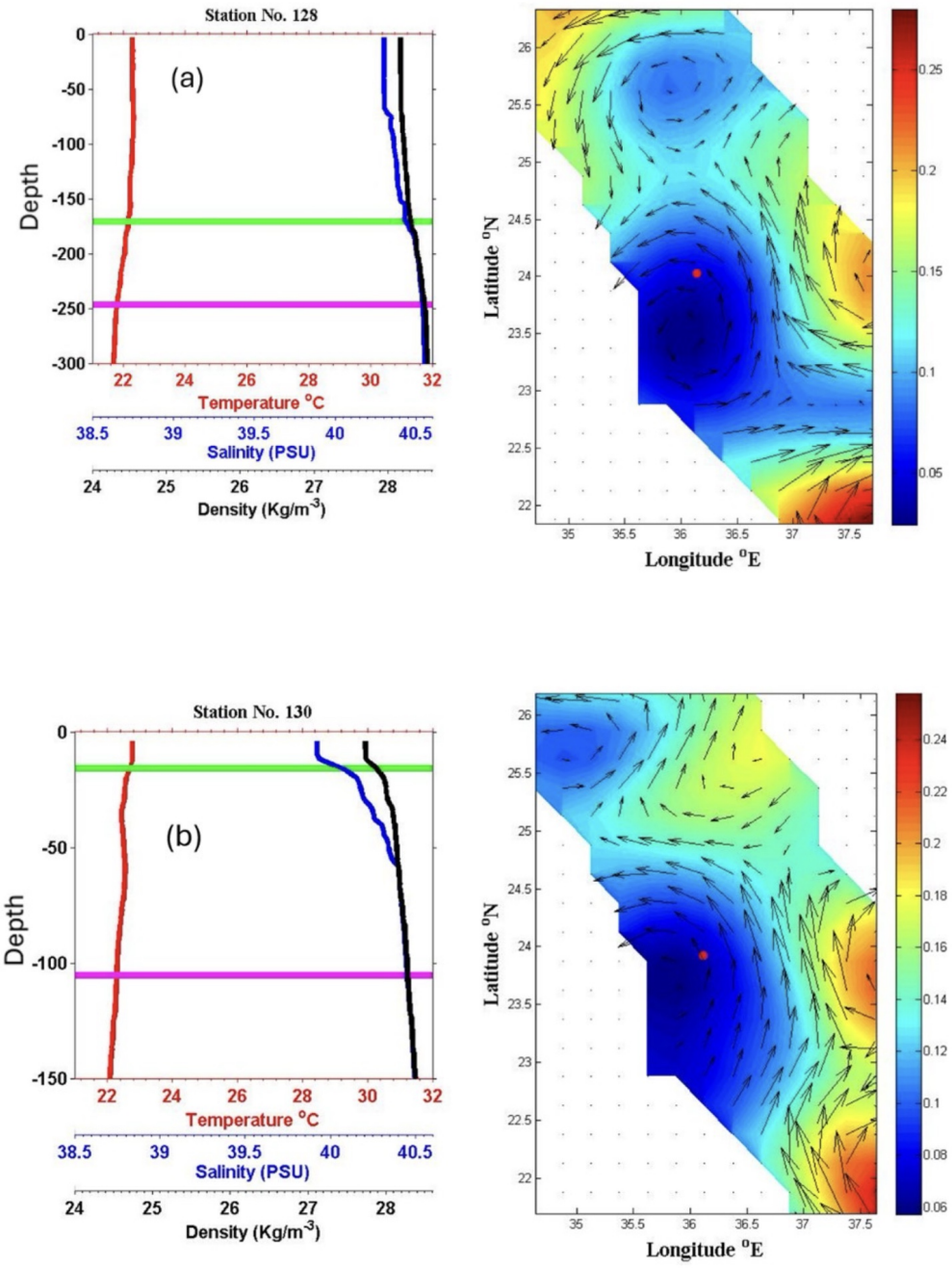

Figure 12. Profiles of temperature, salinity and density from Argo stations no. 128 on February 27, 2017 (a), and station no. February 27, 2017 (b). Both stations are located in the northern of the Red Sea. A magneta line represents MLT green line represents MLD, and their difference represents the BL. SLA maps of the same date is plotted to the right of each pannel CE and AE. Station locations are indicated by red dots.

The analysis compares Argo float observations with the locations of CEs and AEs, identified using SLA data. Eddy activity is most intense in the northern and central regions, particularly north of 18°N, where the long-lived eddies predominantly form between 18°N and 24°N. These eddies are driven by strong wind stress curls associated with seasonal wind jets along the northwestern Red Sea coast. These winds promote enhanced evaporation, surface heat loss, and deep water convection thereby playing a key role in eddy generation and persistence (Zhan et al., 2014; Zhan et al., 2019).

Case observations

Tracking data from Argo floats reveals a clear relationship between eddy activity and the presence of the BL. Observations indicate that the BL tends to weaken or disappear during periods of intensified eddy activity and, re-forms as eddy intensity decreases. A well-defined BL is typically observed in the inter-eddy regions, commonly referred to as the 'background flow' which represents the surrounding water mass outside the eddy core (Rudzin et al., 2017). The BL tends to be thicker within AEs as shown in (Figure 10a) for the central region and (Figure 10b) for the northern region, whereas it is largely absent within CEs (Figure 10c).

Figure 11 shows vertical section of temperature and salinity in the central region. The primary impacts of AEs and CEs are expressed as downward bending of the thermocline and deepening of the mixed layer, accompanied by BL formation under AE conditions (Figure 11a), and upward bending of the surface layer with a shallower mixed

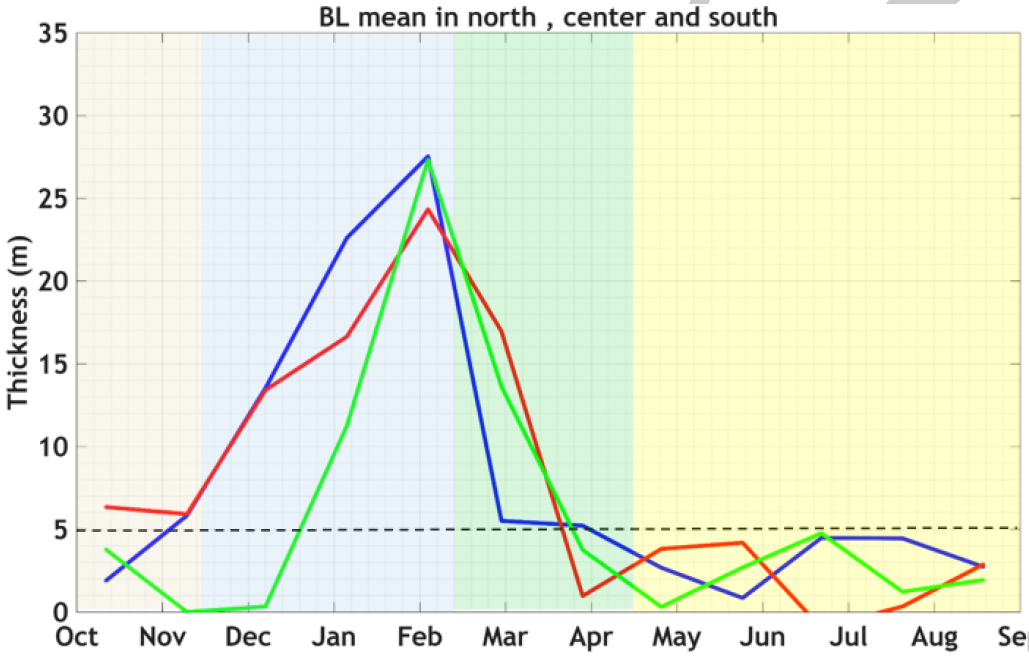

Month		10	11	12	1	2	3	4	5	6	7	8	9	
Season		Autumn		Winter			Spring		Summer					
BL in	N	BL≤ 5m	BL≈ 5m	BL peaks			BL≈ 5m		BL≤ 5m	BL≈ 5m				
	C	BL≈ 5m	BL peaks					BL≤ 5m	BL≈ 5m			BL≤ 5m	BL≈ 5m	
	S	BL≈ 5m	BL≤ 5m	BL≈ 5m	BL peaks			BL≈ 5m	BL≤ 5m	BL≈ 5m		BL≤ 5m	BL≈ 5m	
Wind pattern	N	NNW		High NNW			NNW		Low NNW					
	C	NNW		High NNW			NNW		Low NNW		Tocar gap	Low NNW		
	S	Transitional month	SSE	High SSE NNW convergent with SSE at 16-18°N			SSE	Transitional month	Low NNW				Transitional month	
Water Exchange pattern	N	Most of the GASW sinks at 24° and RSDW form							Most of GAIW sinks at 24°N					
	C	GASW become denser							The GAIW become denser					
	S	Winter two-layer pattern appear							Summer three-layer pattern appear					

Figure 13. Seasonal cycle of monthly mean BL thickness for each region, with different seasons shaded in the plot. The accompanying table summarizes seasonal wind patterns and the associated exchange flow of water for each region during all seasons.

layer and absence of the BL during CE conditions (Figure 11b). These results are consistent with previous findings by Gaube et al. (2019) and He et al. (2020) which indicate that convergence and downwelling within AEs contribute to BL thickening . This provides additional evidence that anticyclonic eddies enhance BLT. Additionally, Rudzin et al. (2017) showed that water properties inside eddies differ from those in the background flow, which may further contribute to BL deepening.

In the northern region, the mixed layer remains deep during winter regardless of the presence of either CEs or AEs. Notably, a pronounced deepening of the surface layer is observed within CEs, contrary to typical expectations, as shown in Figure 12. This discrepancy may be attributed to strong wintertime convective processes in the northern region, which likely outweigh the dynamical influence of cyclonic eddies. This finding is consistent with Yao et al. (2014b), who described a three-dimensional sinking process associated with winter overturning circulation in the northern Red Sea, between 24° and 25°N.

3.6 Seasonal cycle of BLT in the Red Sea

Monthly mean BLT was computed for each region using Argo profiles to characterize the seasonal cycle in the Red Sea. Time series of monthly mean BLT are presented together with schematic representations of the associated wind patterns and exchange flow through the Bab al-Mandeb Strait. We revealed that BL reaches its maximum thickness during winter in all regions (Figure 13). Our findings also revealed pronounced regional differences in BL behavior. In the northern region, the BL is deepest during winter compared with the other regions, whereas it is shallowest in the southern region during the same season. In the central region, the Bl persists for the longest duration, extending from autumn through spring. In contrast, the southern region exhibits the shortest BL duration, with BL presence confined mainly to winter and early spring. During the winter season, strong wind forcing enhances surface buoyance loss, increasing water density and promoting a deep mixed layer, as summarized in the accompanying table. In contrast, weaker winds during summer, combined with surface warming, result in a shallower mixed layer; consequently, the BL is largely absent during this season. The circulation pattern and exchange of water masses between the Red Sea and Gulf of Aden through the Bab al-Mandab Strait also influence the spatial and temporal variability of BLT, as discussed in the Results section.

4. Conclusion

In this study the existence of the BL in the Red Sea is investigated based on Argo float profiles for the period 2012–2018 combined with satellite derived sea level anomaly data. The study area was divided into three regions – the northern (26° to 22°), central (22° to 18°), and southern (18° to 14°) Red Sea – to assess the spatial and temporal variability of the BL. BL evolution was categorized into three seasonal stages: a formation phase during autumn (October–November), a growth phase during winter (December–February) and a decay phase during spring (March–April) and summer (May–September).

This study provides the first confirmation of the presence of a BL in the Red Sea. The spatial and temporal variability of the BL is closely linked to MLD and MLT variations, as BL thickness represents the difference between these two layers. The BL typically develops during winter when BL thickness reaches its maximum in January–February, weakens during spring, and is almost absent during summer.

Significant differences in BL thickness are observed among the northern, central, and southern regions The BL is thickest and deepest in the northern region, where wintertime cooling, strong evaporation and anticyclonic deepening of the MLT relative to the MLD. The central region exhibits intermediate BL thickness, with a long seasonal duration extending from autumn to spring, whereas the southern region displays the thinnest and shortest-lived BL. In all regions haline stratification at the base of the mixed layer plays a key role in BL formation, as indicated by local maxima in the salinity contribution to the buoyancy frequency N_S^2.

SLA data and Argo trajectories were used to examine the impact of AEs and CEs on BL variability in the central and northern Red Sea during winter The analysis revealed that AEs in the central region support thicker BLs through convergence and downwelling within eddy cores, whereas cyclonic eddies shoal the mixed layer and suppress BL formations within CEs. However, in the northern Red Sea mixed layers remain deep during winter even within cyclonic eddies, due to the dominance of strong wintertime convective overturning.

Density compensated layers associated with temperature inversions are observed in the central and southern Red Sea and may influence heat and freshwater exchange at the base of the mixed layer, these features were not analyzed in the present study.

Acknowledgements

H.A. acknowledges the support of former HOD Prof. Abdullah Al-Subhi and Dr. Rana Alghamdi and for their valuable feedback and assistance in reviewing the manuscript. The authors acknowledge the Coriolis Data Center and the E.U. Copernicus Marine Service Information for making their data products publicly available.

Conflict of interest

None declared.

Supplementary material

Supplementary material associated with this article can be found here.

References

Abdulla, C. P., Alsaafani, M. A., Alraddadi, T. M., Albarakati, A. M., 2018. *Mixed layer depth variability in the Red Sea*. Ocean Sci. 14(4), 563–573. https://doi.org/10.5194/os-14-563-2018

Al Saafani, M. A., Shenoi, S. S. C., 2004. *Seasonal cycle of hydrography in the Bab el Mandab region, southern Red Sea*. J. Earth Syst. Sci. 113, 269–280. https://doi.org/10.1007/BF02716725

Balaguru, K., Chang, P., Saravanan, R., Jang, C. J., 2012. *The barrier layer of the Atlantic warmpool: formation mechanism and influence on the mean climate*. Tellus A: Dynam.Meteorol. Oceanogr. 64(1). https://doi.org/10.3402/tellusa.v64i0.18162

Balaguru, K., Chang, P., Saravanan, R., Leung, L. R., Xu, Z., Li, M., Hsieh, J. S., 2012. *Ocean barrier layers' effect on tropical cyclone intensification*. https://doi.org/10.1073/pnas.1201364109 Proc. Nat. Acad. Sci. 109(36), 14343–14347.

Bower, A.S., Farrar, J.T., 2015. *Air-sea interaction and horizontal circulation in the Red Sea*. [In:] Rasul, N., Stewart, I. (eds.) *The Red Sea*. Springer Earth System Sciences. Springer, Berlin, Heidelberg. https://doi.org/10.1007/978-3-662-45201-1_19

Cabrera, O. C., Villanoy, C. L., David, L. T., Gordon, A. L., 2011. *Barrier layer control of entrainment and upwelling in the Bohol Sea, Philippines*. Oceanography 24(1), 130–141. http://www.Jstor.Org/Stable/24861246

Cronin, M. F., McPhaden, M. J., 2002. *Barrier layer formation during westerly wind bursts*. J. Geophys. Res.-Oceans 107(C12), SRF-21. https://doi.org/10.1029/2001JC001171

De Boyer Montégut, C., Mignot, J., Lazar, A., Cravatte, S., 2007. Control of salinity on the mixed layer depth in the world ocean: 1. General description. J. Geophys. Res.-Oceans 112(C6). https://doi.org/10.1029/2006JC003953

Dong, S., Goni, G., Lumpkin, R., 2015. *Mixed-layer salinity budget in the SPURS region on seasonal to interannual time scales.* Oceanography 28(1), 78–85. http://www.jstor.org/stable/24861845

Durand, F., Shankar, D., de Boyer Montégut, C., Shenoi, S. S. C., Blanke, B., Madec, G., 2007. *Modeling the barrier-layer formation in the southeastern Arabian Sea*. J. Climate 20(10), 2109–2120. https://doi.org/10.1175/JCLI4112.1

Echols, R., Riser, S. C., 2020. *The impact of barrier layers on Arabian Sea surface temperature variability*. Geophys. Res. Lett. 47(3), e2019GL085290. https://doi.org/10.1029/2019GL085290

Foltz, G. R., McPhaden, M. J., 2009. *Impact of Barrier Layer Thickness on SST in the Central Tropical North Atlantic*. J. Clim. 22(2), 285–299. https://doi.org/10.1175/2008JCLI2308.1

Gaube, P. J., McGillicuddy Jr, D., Moulin, A. J., 2019. *Mesoscale eddies modulate mixed layer depth globally*. Geophys. Res. Lett. 46(3), 1505–1512. https://doi.org/10.1029/2018GL080006

Gayan Pathirana, U. P., Chen, G., Priyadarshana, T., Wang, D., 2017. *Importance of vertical mixing and barrier layer variation on seasonal mixed layer heat balance in the Bay of Bengal*. Ocean Sci. Discuss. 2017, 1–27. https://doi.org/10.5194/os-2017-67

George, J. V., Vinayachandran, P. N., Vijith, V., Thushara, V., Nayak, A. A., Pargaonkar, S. M., Amol, P., Vijaykumar, K., Matthews, A. J., 2019. *Mechanisms of Barrier Layer Formation and Erosion from In Situ Observations in the Bay of Bengal*. J. Phys. Oceanogr. 49(5), 1183–1200. https://doi.org/10.1175/JPO-D-18-0204.1

Girishkumar, M. S., Ravichandran, M., McPhaden, M. J., 2013. *Temperature inversions and their influence on the mixed layer heat budget during the winters of 2006–2007 and 2007–2008 in the Bay of Bengal*. J. Geophys. Res.-Oceans 118(5), 2426–2437. https://doi.org/10.1002/jgrc.20192

Hansen, D. V., Thacker, W. C., 1999. *Estimation of salinity profiles in the upper ocean*. J. Geophys. Res.-Oceans 104(C4), 7921–7933. https://doi.org/10.1029/1999JC900015

He, Q., Zhan, H., Cai, S., 2020. *Anticyclonic eddies enhance the winter barrier layer and surface cooling in the Bay of Bengal*. J. Geophys. Res.-Oceans, 125(10), e2020JC016524. https://doi.org/10.1029/2020JC016524

Head, S. M., Edwards, A. J. (Eds.), 1987. *Red Sea*. Pergamon Press. https://www.academia.edu/download/82710153/Frazier_1987_Red_Sea_Turtles_and_marine_mammals.pdf

Jones, E. N., Browning, D. G., 1971. *Cold water layer in the southern Red Sea*. Limnol. Oceanograph. 16(3), 503–509. https://doi.org/10.4319/lo.1971.16.3.0503

Kantha, L., Clayson, C. A., 2003. *Ocean mixed layer*. Encyclop. Atmos. Sci., 291–298. https://doi.org/10.1016/B0-12-227090-8/00093-2

Krokos, G., Cerovečki, I., Zhan, P., Hendershott, M. C., Hoteit, I., 2021. *Seasonal evolution of mixed layers in the Red Sea and the relative contribution of atmospheric buoyancy and momentum Forcing*. arXiv preprint arXiv:2112.08762. https://doi.org/10.48550/arXiv.2112.08762

Langodan, S., Cavaleri, L., Vishwanadhapalli, Y., et al., 2017. *The climatology of the Red Sea – part 1: the wind*. Int. J. Climatol. http://dx.doi.org/10.1002/joc.5103

Langodan, S., Cavaleri, L., Viswanadhapalli, Y., Hoteit, I., 2014. *The Red Sea: a natural laboratory for wind and wave modeling*. J. Phys. Oceanogr.44(12), 3139–3159. https://doi.org/10.1175/JPO-D-13-0242.1

Liu, H., Grodsky, S. A., Carton, J. A., 2009. *Observed subseasonal variability of oceanic barrier and compensated layers*. J. Clim. 22(22), 6104–6119. https://doi.org/10.1175/2009JCLI2974.1

Lukas, R., Lindstrom, E., 1991. *The mixed layer of the western equatorial Pacific Ocean*. J. Geophys.Res.-Oceans 96(S01), 3343–3357. https://doi.org/10.1029/90JC01951

Mackey, D. J., Parslow, J., Higgins, H. W., Griffiths, F. B., O'Sullivan, J. E., 1995. *Plankton productivity and biomass in the western equatorial Pacific: biological and physical controls*. Deep Sea Res. Pt. II: Topical Stud. Oceanogr. 42(2–3), 499–533. https://doi.org/10.1016/0967-0645(95)00038-R

Maes, C., Belamari, S., 2011. *On the impact of salinity barrier layer on the Pacific Ocean mean state and ENSO*. Sola 7, 97–100. https://doi.org/10.2151/sola.2011-025

Maes, C., O'Kane,T. J., 2014. *Seasonal variations of the upper*

Marshall, D., 1997. *Subduction of water masses in an eddying ocean*. https://elischolar.library.yale.edu/journal_of_marine_research/2223

Mignot, J., de Boyer Mont égut, C., Tomczak, M., 2009. *On the porosity of barrier layers*. Ocean Sci. 5(3), 379–387. https://doi.org/10.5194/os-5-379-2009

Mignot, J., de Boyer Montégut, C., Lazar, A., Cravatte, S., 2007. *Control of salinity on the mixed layer depth in the world ocean: 2. Tropical areas*. J. Geophys. Res.-Oceans, 112(C10). https://doi.org/10.1029/2006JC003954

Mohleji, S., Clayson, C. A., 13.6 precipitation variability and barrier-layer formation in the north indian ocean. https://ams.confex.com/ams/pdfpapers/35639.pdf

Morcos, S. A., 1970. *Physical and chemical oceanography of the Red Sea*, Oceanogr. Mar. Biol. Annu. Rev. 8, H. Barnes, 73–202.

Murray, S. P., Johns, W., 1997. *Direct observations of seasonal exchange through the Bab el Mandab Strait*. Geophys. Res. Lett. 24(21), 2557–2560. https://doi.org/10.1029/97GL02741

Maes, C., O'Kane, T. J., 2014. *Seasonal variations of the upper ocean salinity stratification in the tropics*. J. Geophys. Res.-Oceans 119 (3), 1706–1722 https://doi.org/10.1002/2013JC009366

Pailler, K., Bourls, B., Gouriou, Y., 1999. *The barrier layer in the western tropical Atlantic Ocean*. Geophys. Res. Lett. 26(14), 2069–2072. https://doi.org/10.1029/1999GL900492

Pan, A., Liang, C., Wan, X., 2019. *Features, Mechanism of the Barrier Layer in the Tropical Pacific Ocean and its Relationship with ENSO*. Examines Mar. Biol. Oceanogr. 3(2). https://doi.org/10.31031/EIMBO.2019.03.000556

Pan, L., Zhong, Y., Liu, H., Zhou, L., Zhang, Z., Zhou, M., 2018. *Seasonal variation of barrier layer in the Southern Ocean*. J. Geophys. Res.-Oceans 123(3), 2238–2253. https://doi.org/10.1002/2017JC013382

Qu, T., Meyers, G., 2005. *Seasonal variation of barrier layer in the southeastern tropical Indian Ocean*. J. Geophys. Res.-Oceans 110(C11). https://doi.org/10.1029/2004JC002816

Radenac, M. H., Rodier, M., 1996. *Nitrate and chlorophyll distributions in relation to thermohaline and current structures in the western tropical Pacific during 1985–1989*. Deep-Sea Res. Pt. II: Topical Stud. Oceanogr 43(4–6), 725–752. https://doi.org/10.1016/0967-0645(96)00025-2

Radenac, M. H., Messié, M., Léger, F., Bosc, C., 2013. *A very oligotrophic zone observed from space in the equatorial Pacific warm pool*. Remote Sens. Environ. 134, 224–233. https://doi.org/10.1016/j.rse.2013.03.007

Rao, R. R., Sivakumar, R., 2003. *Seasonal variability of sea surface salinity and salt budget of the mixed layer of the north Indian Ocean*. J. Geophys. Res.-Oceans 108(C1), 9–11. https://doi.org/10.1029/2001JC000907

Ruardij, P., Van Haren, H., Ridderinkhof, H., 1997. *The impact of thermal stratification on phytoplankton and nutrient dynamics in shelf seas: a model study*. J. Sea Res. 38(3–4), 311–331. https://doi.org/10.1016/S1385-1101(97)00042-7

Rudzin, J. E., Shay, L. K., Jaimes, B., Brewster, J. K., 2017. *Upper ocean observations in eastern C aribbean S ea reveal barrier layer within a warm core eddy*. J. Geophys. Res.-Oceans122(2), 1057–1071. https://doi.org/10.1002/2016JC012339

Shanas, P. R., Aboobacker, V. M., Albarakati, A. M., Zubier, K. M., 2017. *Climate driven variability of wind-waves in the Red Sea*. Ocean Model. 119, 105–117. https://doi.org/10.1016/j.ocemod.2017.10.001

Shenoi, S. S. C., Shankar, D., Shetye, S. R., 2002. *Differences in heat budgets of the near-surface Arabian Sea and Bay of Bengal: Implications for the summer monsoon*. J. Geophys. Res.-Oceans 107(C6), 5–11. https://doi.org/10.1029/2000JC000679

Shenoi, S. S. C., Shankar, D., Shetye, S. R., 2004. *Remote forcing annihilates barrier layer in southeastern Arabian Sea*. Geophys. Res. Lett. 31(5). https://doi.org/10.1029/2003GL019270

Silva, A., Araujo, M., Medeiros, C., Silva, M., Bourles, B., 2005. *Seasonal changes in the mixed and barrier layers in the western equatorial Atlantic*. Brazilian J. Oceanogr. 53, 83–98. https://www.scielo.br/j/bjoce/a/Gtt9H7qnKVRJvhHhdch6NJy/

Sofianos, S. S., Johns, W. E., 2003. *An oceanic general circulation model (OGCM) investigation of the Red Sea circulation: 2. Three-dimensional circulation in the Red Sea*. J. Geophys. Res.-Oceans 108(C3). https://doi.org/10.1029/2001JC001185

Sofianos, S., Johns, W.E., 2015. *Water mass formation, Ooverturning circulation, and the exchange of the Red Sea with the adjacent basins*. [In:] Rasul, N., Stewart, I. (eds.), *The Red Sea*. Springer Earth Sys.Sci. Springer, Berlin, Heidelberg https://doi.org/10.1007/978-3-662-45201-1_20

Sprintall, J., Cronin, M. F., 2001. *Upper ocean vertical structure*. https://doi.org/10.1006/rwos.2001.0149

Sprintall, J., Tomczak, M., 1992. *Evidence of the barrier layer in the surface layer of the tropics*. J. Geophys. Res.-Oceans 97(C5), 7305–7316. https://doi.org/10.1029/92JC00407

Thadathil, P., Muraleedharan, P. M., Rao, R. R., Somayajulu, Y. K., Reddy, G. V., Revichandran, C., 2007. *Observed seasonal variability of barrier layer in the Bay of Bengal*. J. Geophys. Res.-Oceans 112(C2). https://doi.org/10.1029/2006JC003651

Thadathil, P., Thoppil, P., Rao, R. R., et al., 2008. *Seasonal variability of the observed barrier layer in the Arabian Sea*. J. Phys. Oceanogr. 38(3), 624–638. https://doi.org/10.1175/2007JPO3798.1

Vialard, J., Delecluse, P., 1998. *An OGCM study for the TOGA decade. Pt. I: Role of salinity in the physics of the western Pacific fresh pool*. J. Phys. Oceanogr. 28(6), 1071–1088. https://doi.org/10.1175/1520-0485(1998)028<1071:AOSFTT>2.0.CO;2

Yao, F., Hoteit, I., Pratt, L. J., Bower, A. S., Zhai, P., Köhl, A., Gopalakrishnan, G., 2014. *Seasonal overturning circulation in the Red Sea: 1. Model validation and summer circulation*. J. Geophys. Res.-Oceans 119(4), 2238–2262. https://doi.org/10.1002/2013JC009004

Yao, F., Hoteit, I., Pratt, L. J., Bower, A. S., Köhl, A., Gopalakrishnan, G., Rivas, D., 2014b. *Seasonal overturning circulation in the Red Sea: 2. Winter circulation*. J. Geophys. Res.-Oceans 119(4), 2263–2289. https://doi.org/10.1002/2013JC009331

Zarokanellos, N. D., Kürten, B., Churchill, J. H., Roder, C., Voolstra, C. R., Abualnaja, Y., Jones, B. H., 2017. *Physical mechanisms routing nutrients in the central Red Sea*. J. Geophys. Res.-Oceans 122(11), 9032–9046. https://doi.org/10.1002/2017JC013017

Zeng, L., Wang, D., 2017. *Seasonal variations in the barrier layer in the South China Sea: characteristics, mechanisms and impact of warming*. Climate Dynam. 48(5), 1911–1930. https://doi.org/10.1007/s00382-016-3182-8

Zhai, P., Bower, A., 2013. *The response of the Red Sea to a strong wind jet near the Tokar Gap in summer*. J. Geophys. Res.-Oceans 118(1), 421–434. https://doi.org/10.1029/2012JC008444n

Zhan, P., Krokos, G., Guo, D., Hoteit, I, 2019. *Three-dimensional signature of the Red Sea eddies and eddy-induced transport*. Geophys. Res. Lett. 46(4), 2167–2177. https://doi.org/10.1029/2018GL081387

Zhan, P., Subramanian, A. C., Yao, F., Hoteit, I., 2014. *Eddies in the Red Sea: A statistical and dynamical study*. J. Geophys. Res.-Oceans 119(6), 3909–3925. https://doi.org/10.1002/2013JC009563